Specific Absorption Rate and Current Densities in the Human Eye and Head Induced by the Telemetry Link of an Epiretinal Prosthesis

Vinit Singh, *Student Member, IEEE*, Amit Qusba, Arup Roy, Richard A. Castro, Kelly McClure, *Member, IEEE*, Rongching Dai, *Member, IEEE*, Robert J. Greenberg, *Member, IEEE*, James D. Weiland, *Senior Member, IEEE*, Mark S. Humayun, *Member, IEEE*, and Gianluca Lazzi, *Fellow, IEEE*

***Abstract*—The fields induced in the human head by the wireless telemetry used for Second Sight Medical Product, Inc.'s epiretinal prosthesis system are characterized for compliance testing with international safety standards using a three-dimensional (3-D) finite-difference time-domain (FDTD) code in D-H formulation. The specific system under consideration utilizes an inductive link with a primary coil mounted on the subject's eyeglasses and a secondary coil that is strapped on the eye, over the sclera. The specific absorption rate (SAR) and the current density have been obtained computationally for different relative positions of the primary and secondary coils to account for the relative misalignment of the two due to the movement of the eye with the implant. For a peak normalized current of 0.62 A in the primary coil at 10 MHz, the highest peak 1-g SAR was found to be 0.45 W/Kg, and the maximum root mean square (rms) current density averaged over a 1-cm ^{2} area was found to be 16.05 A/m^2, both of which are within the limits imposed by IEEE and ICNIRP safety standards. Simulations between 2 and 20 MHz indicated that the induced electric field values scale well with frequency, thus providing guidelines for the determination of the final frequency and input power requirements of operation for the telemetry system to meet safety standards.**

***Index Terms*—Bioelectromagnetics, finite-difference time-domain (FDTD), specific absorption rate (SAR).**

I. Introduction

RETINITIS PIGMENTOSA (RP) and age-related macular degeneration (AMD) are retinal degenerative diseases leading to partial or complete blindness affecting approximately 10 million people worldwide. Extensive research is being carried out [1]–[4] with different approaches to develop a rehabilitative device to restore partial sight to patients affected by these illnesses. While a number of approaches to the stimulation of the surviving neural cells in the retina have been proposed, our present work deals specifically with the dual-unit epi-retinal approach [1], [2], where the target cells for stimulation are the surviving ganglion and bipolar cells.

To minimize the number of internal components, it is proposed to keep most of the signal processing units outside the body. Thus, a wireless telemetry system is necessary to provide power and data to the implanted stimulator chip that drives the micro-electrodes responsible for exciting the underlying ganglion cells.

Before surgical implantation of the internal components, it is imperative to perform a thorough safety analysis (using simulation, human phantoms, laboratory animals) of the possible harmful effects to the tissues. One possible cause of these effects is heat generation, whose sources are the stimulator chip, the electrode array, power dissipated in the secondary coil, and the electromagnetic power absorbed in the tissues due to the telemetry link.

A detailed discussion of the thermal effects of bio-implants can be found in [5]. Specifically, a thorough treatment of the thermal effects of the stimulator chip and the secondary coil for this particular prosthesis system has been carried out in another publication [6]. The current generation of the prosthesis design by Second Sight Medical Products (SSMP), Inc., under clinical trials is the ArgusII, a 60-electrode device. As the electrode count increases, the power requirements and the ensuing heat generated may become the primary issues for such devices.

Another possible unwanted effect due to the telemetry system is parasitic neuronal stimulation. A human body cell membrane (which conveys the neural signals) behaves like a capacitor, which becomes progressively less responsive with increasing frequency. Extensive studies have shown that strong, inductive, low-frequency (up to a few hundred kHz) fields have the capability to excite nerves directly causing undesirable physiological effects [7]. Furthermore, even a subthreshold but substantial chronic stimulation can adversely affect the activity of the central nervous system [7]. However, above 10 MHz, the exposure restrictions are dictated by tissue heating via energy deposition rather than stimulation.

Some earlier investigation of the electromagnetic effects [only specific absorption rate (SAR)] of the retinal prosthesis was carried out in [8], [9] for a two-dimensional (2-D) head

Manuscript received October 12, 2007; revised February 10, 2009. First published July 28, 2009; current version published October 07, 2009. This work was supported in part by the Office of Science (BER), U.S. Department of Energy under Grant ER63752-1022761-0009747 and in part by the NSF under Grant EEC-0310723.

V. Singh, A. Qusha, and G. Lazzi are with the Department of Electrical and Computer Engineering, North Carolina State University, Raleigh, NC 27695-7914 USA (e-mail: lazzi@eos.ncsu.edu).

A. Roy, R. A. Castro, K. McClure, R. Dai, and R. J. Greenberg are with Second Sight Medical Products, Inc., Sylmar, CA 91342 USA.

J. D. Weiland and M. S. Humayun are with the Doheny Eye Institute, Keck School of Medicine, University of Southern California, Los Angeles, CA 90089 USA.

Color versions of one or more of the figures in this paper are available online at http://ieeexplore.ieee.org.

Digital Object Identifier 10.1109/TAP.2009.2028498

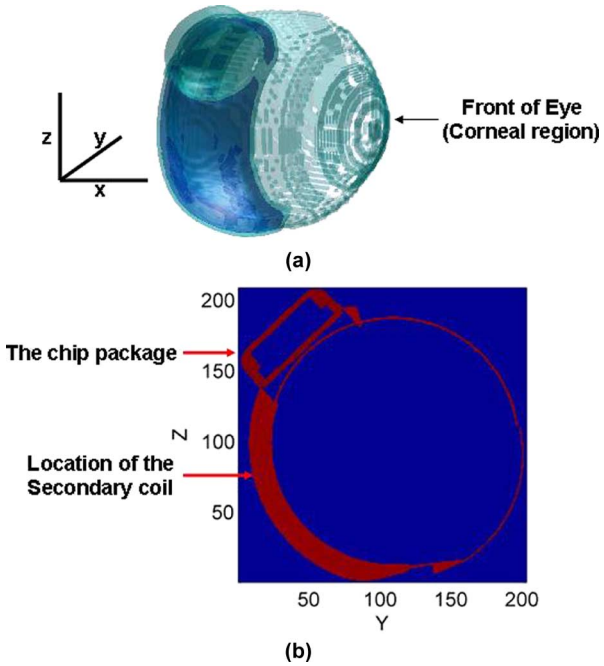

Fig. 1. (a) The intended position of the implant placed on the eye. The broad flat portion encloses the secondary coil, while the chip package is near the top (along the z-axis). (b) A cross section (along the y-z plane) through the implant and eye (in the region inside the implant) are not shown here.

TABLE I
CONDUCTIVITY OF KEY TISSUES AT DIFFERENT FREQUENCIES

Tissue	Conductivity (Sm^{-1})				
	2 MHz	5 MHz	10 MHz	15 MHz	20 MHz
Muscle	0.55	0.59	0.62	0.63	0.64
Sclera	0.69	0.76	0.8	0.82	0.83
Skin	0.04	0.11	0.2	0.25	0.29
Retina	0.69	0.76	0.8	0.82	0.83
Vitreous Humor	1.5	1.5	1.5	1.5	1.5

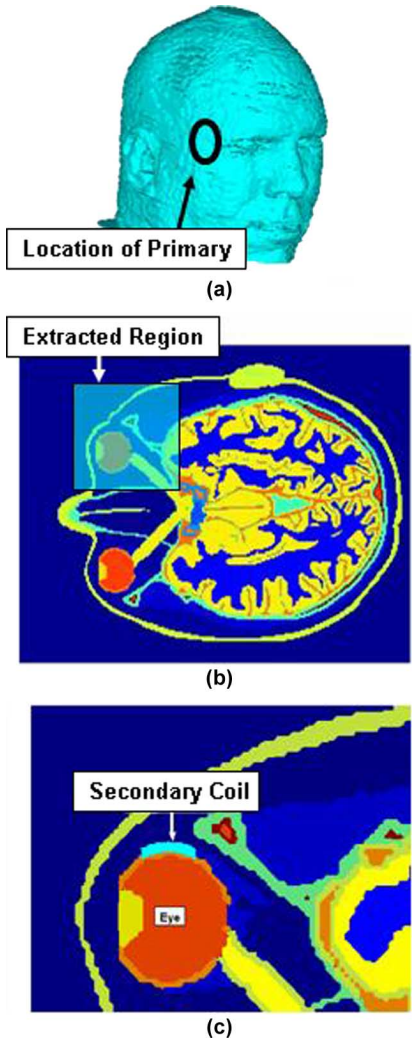

Fig. 2. (a) A 3-D model of the head and the approximate location of the primary coil. (b) Slice of the human head indicating the extracted region for the FDTD simulations. (c) The extracted model with the implanted secondary coil. The size of the computational space of the extracted region at 0.3 mm resolution was $180 \times 240 \times 200$.

model at 2 MHz and for a three-dimensional (3-D) head model at 10 MHz [10]. However, in both, the primary coil was modeled as a single loop. This work differs from the previous work on the following accounts. First, the actual spiral primary coil and implanted components used in the current prototype implant and derived from CAD files have been discretized and merged with the head model. Second, the primary coil is mounted on the patient's eyeglasses and positioned on the side of the eye parallel to the forehead, while the secondary coil is strapped on the eye, over the sclera. Third, induced current densities have also been computed. Fourth, different orientations and distances of the primary coil have been considered for different frequencies for a more comprehensive characterization of the electromagnetic effects of the system.

Typically used numerical methods for problems like this are based on either the finite-difference time-domain (FDTD) method or the finite-element method (FEM). FEM has the advantage of being able to resolve curved contours very well as compared to FDTD. However, there exist two fundamental reasons that make FDTD a preferred scheme for this problem. The primary reason for using FDTD is the requirement of high-resolution models of the human head/eye that are readily available in voxelized format [8], [11]. Since the prosthesis components (internal and external to the body) were to be integrated with the head model at 0.3 mm, discretizers were used to convert the CAD drawings to required formats. As shown in the paper, the FDTD model provides a fairly accurate model when compared to analytically computed values and experimental measurements. The second reason for the choice of FDTD is the usually smaller memory requirements for this problem at the given uniform resolution required to adequately describe the eye tissues and the implant materials.

This paper consists of six sections. Section II describes the head model used. This is followed by a discussion, in Section III, of the different orientations of the primary coil with respect to the head considered in this paper. In Section IV, a detailed discussion of the method of excitation is provided. The results are presented in Section V, followed by a discussion and concluding remarks in Section VI.

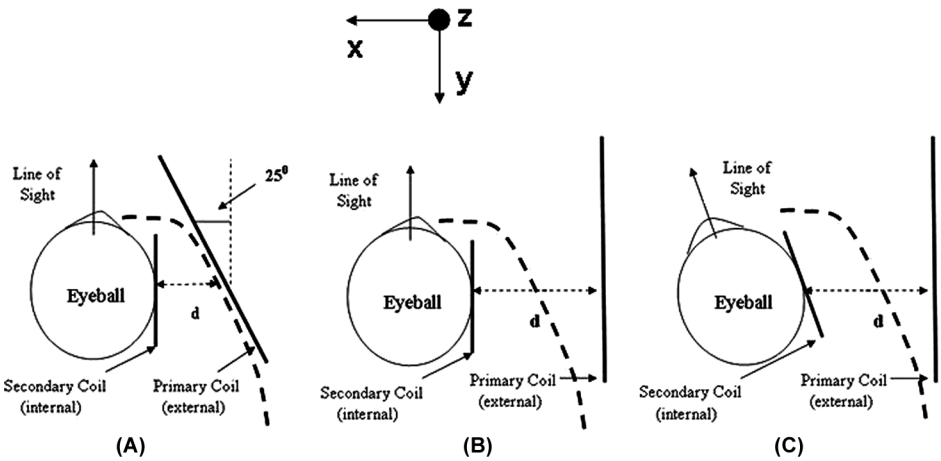

Fig. 3. The different orientations of the eye and primary coil considered. The curved dashed line indicates roughly the head contour at the cross section.

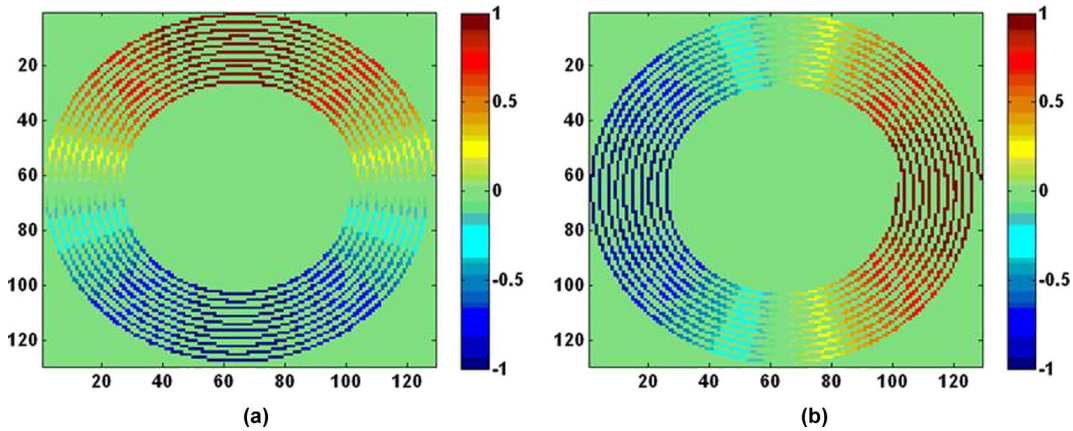

Fig. 4. Normalized magnitude and direction (indicated by sign on the colorbar) of the (a) y- and (b) z-components of the D-field. Since the current in the coil is directly proportional to the D-field, its distribution will be identical.

II. Head and Implant Models

The implant and primary coil models were imported from CAD file formats, discretized, and incorporated in the head model. Fig. 1 shows a discretized model of the eye with the implant positioned on its curvature. The implant is to be held in places via scleral straps wrapping around the eye. The dielectric properties of the tissues at different frequencies were obtained from [12]. Table I lists the conductivity of some of the key tissues.

The original model of the human head was obtained in the form of 1-mm resolution slices from the *Visible Man Project* from the National Library of Medicine [11], then rediscretized to a resolution of 0.3 mm using linear interpolators [Fig. 2(a)]. Fig. 2(b) and (c) show a cross section of the original head model and the extracted region used for the simulations.

III. Modeling

It is envisioned that the external components including the primary coil will be placed on a pair of eyeglasses worn by the subject. Based on this, we have investigated the energy absorption and induced currents for different orientations and distances of the primary coil with respect to the forehead near the right eye.

The primary coil position is not expected to be constant during operation, although the position of the secondary coil will be fixed with respect to the eye. Fig. 3 shows the different orientations of the primary coil considered for the simulations. These orientations were used for two distances between the coil and the forehead.

With reference to Fig. 3, position (A) is when the primary is parallel to the forehead. Note that in this position, the primary is inclined toward the secondary coil [refer to Figs. 2(c) and 3(a)]. Position (B) is when the primary is turned away by approximately 25° with the lower end as the pivot in the figure. In this position, the primary and secondary coils are approximately parallel. This leads to a distance slightly larger than that for position (A). The third position (C) is when the eye is rotated by 20° (eye looking left). The distance "d" is about 2.07, 2.8, and 3 cm for (A), (B), and (C), respectively. The simulations for all these three positions were repeated by moving the primary coil along positive-x direction to be almost in contact with the forehead leading to distances of 1.1, 1.6, and 1.85 cm. These are referred to as (A'), (B'), and (C'). Two obvious inferences can be made at the outset. First, the induced E-fields for positions B and C will be very similar since the position of the forehead in unchanged; similarly, positions B' and C' also lead to comparable induced E-fields. Second, the induced E-fields will be

greater for positions $\mathrm{A}', \mathrm{B}',$ and C' compared to those for positions A, B, and C, due to the smaller distance from the primary coil. Note that to ensure that coil voxels are not contiguous with tissue, the location of the primary coil had to be adjusted along *y*- and *z*-directions as well.

The diameter of the primary coil filament is 0.9 mm, and the discretization of its CAD model at 0.3 mm resolution led to a three-cell-thick primary coil. Since rotating the coil model by 25° would lead to disconnects in the discretized model, the head model was rotated by the required angle. For the case where the eyeball is turned, only the eye tissues and the implant are rotated.

IV. Primary Coil: Excitation and Verification

The primary coil is spiral-shaped with external diameter 39 mm and internal diameter 21.5 mm and acts as the power and data source with data modulating the relatively low-frequency power carrier. A current can be excited in one of several ways in the FDTD method. For example, applying a voltage difference using the finite-gap method will force a current through the coil. However, the problem with this excitation with respect to the coil considered in this paper is that at the considered resolution (0.3 mm), the coil turns are not smooth, leading to possible disconnects in the staggered grid, which will affect the integrity of the current in the coil. Another possibility is using the H-field curl around the coil. However, this implicitly assumes that the magnetic field is identical at the points of excitation, which leads to an inaccurate H-field distribution.

In this work, the method used to simulate a current in the coil is a D-field (displacement field) source at each voxel representing the current in it. Assuming the coil is in the *y*-*z* plane and based on a normalized current, D_y and D_z values were assigned to each coil voxel based on the angle made by that cell with the center of the coil. Another reasonable assumption made was that the current magnitude through each voxel was identical. Fig. 4 indicates the D-field magnitudes (normalized to a peak value of 1 A) in the *y*- and *z*-directions.

To verify the excitation, the E-field distribution in the absence of human tissue using FDTD was compared to that obtained using the method described by [13], in which the E-field is calculated at any point, $\mathrm{P}(\overline{r})$ in space due to a current element, dl, using

$$dE = \frac{\mu_0 N (dI/dt)\,\vec{d}\,l}{4\pi R} \tag{1}$$

where R is the distance between the current element and $\mathrm{P}(\overline{r})$, N is the number of turns, and dI/dt is the rate of change of current. The total electric field at the point $\mathrm{P}(\overline{r})$ can then be obtained by integration over the entire coil length. Since we are interested in the peak E-field distribution, $dI/dt = I_{\mathrm{peak}}.\omega$. Fig. 5 compares the E-field distribution obtained using this method and FDTD.

Measurements using an electric field probe and the data acquisition system (DASY) manufactured by SPEAG AG were also performed for the fabricated primary coil in free space to compare with the FDTD results (Fig. 6). Results in Fig. 7 show that relative measured and computed electric field are in good agreement, especially considering the large gradients of the field in close proximity to the coil (Fig. 8).

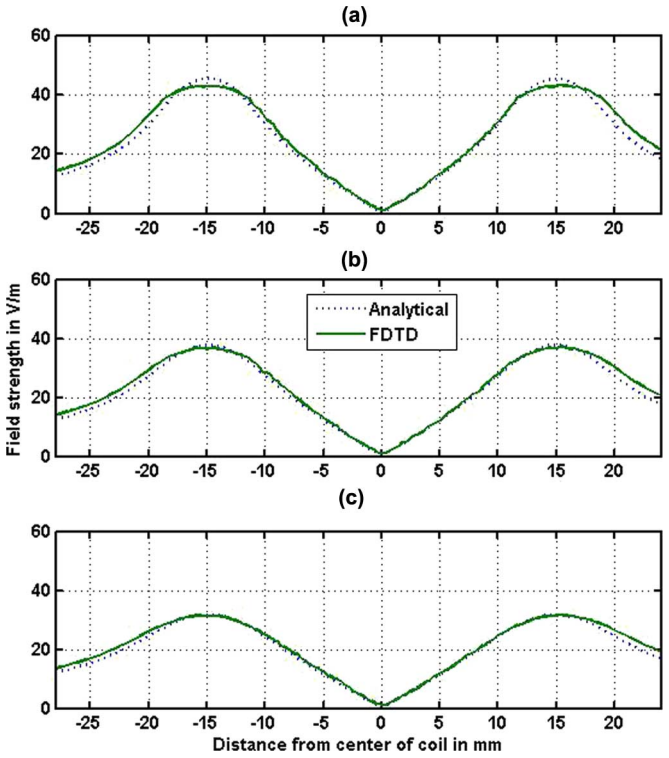

Fig. 5. Analytical and FDTD-computed electric field magnitudes at different distances from the primary coil. Results are in absence of the head model. (a) 1.2 mm from plane of coil; (b) 2.4 mm from plane of coil; (c) 3.6 mm from plane of coil.

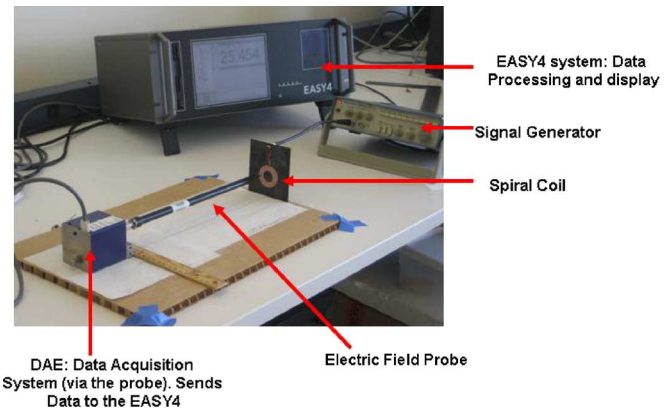

Fig. 6. Experimental setup for the measurement of the electric field in proximity of the primary coil.

A simple well-known formula for the magnetic field intensity along the axis of a concentric current-carrying loop is

$$H = \frac{IR^2}{2\sqrt{(R^2 + x^2)^3}} \tag{2}$$

where I is the current through each filament, x is the distance from the center of the loop along its axis, and R is the mean radius of the coil. For N concentric loops, the H-field could be computed as the sum of the H fields of N single-turn loops of different radii.

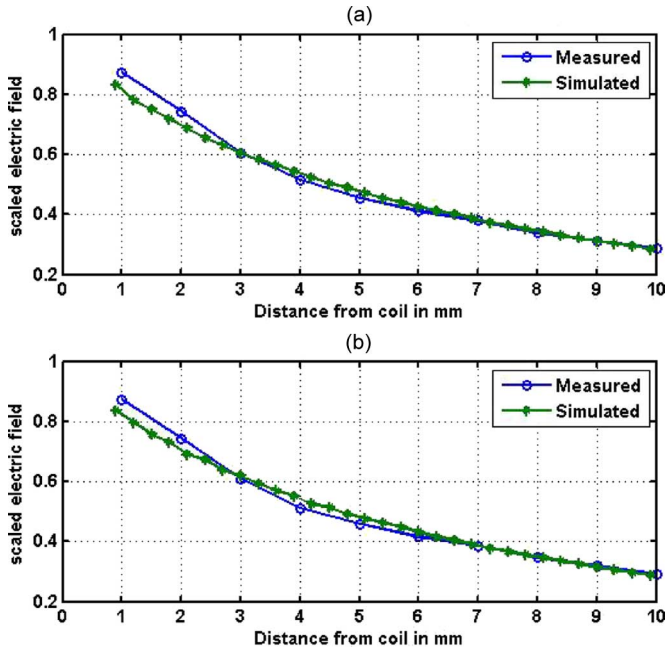

Fig. 7. Normalized measured and simulated electric field along a line perpendicular to the plane of coil. The two graphs correspond to lines that intersect the coil at diametrically opposite points. (a) Perpendicular distance from coil (from edge); (b) distance from diametrically opposite edge.

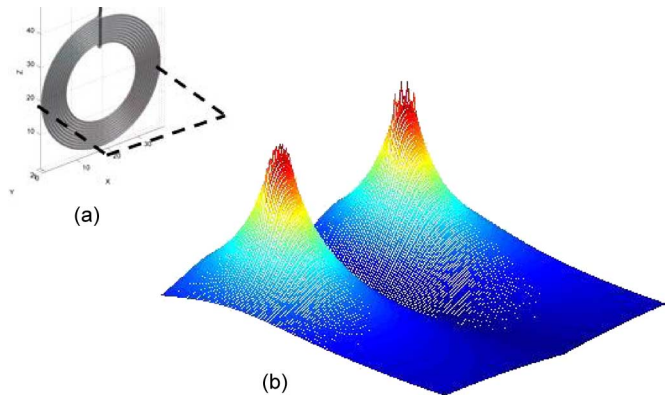

Fig. 8. (a) Primary coil and the plane in which the electric fields are shown. (b) Computed electric field pattern plot illustrating relative large gradients perpendicular and parallel to the coil.

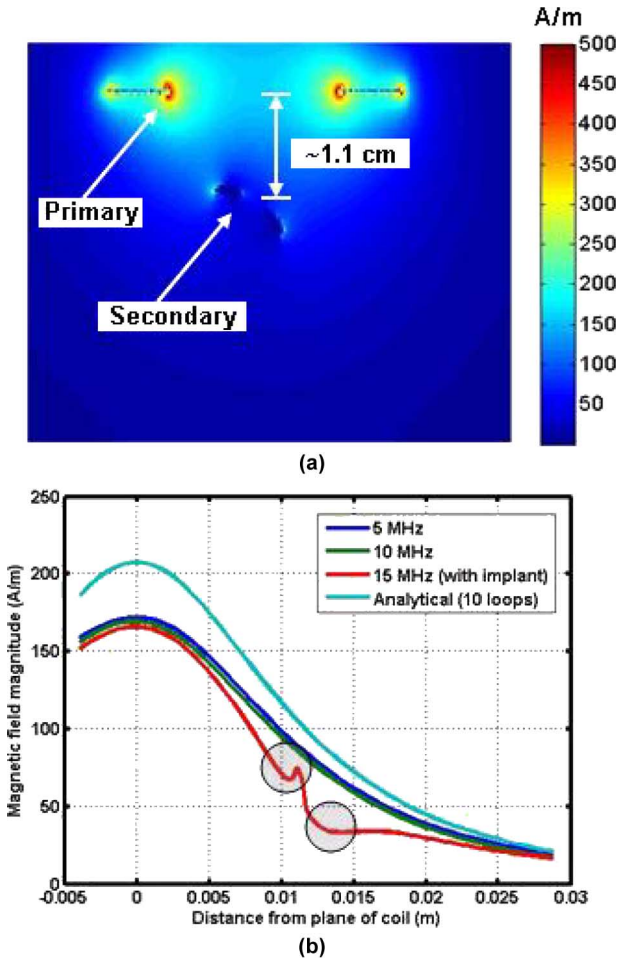

Fig. 9. (a) H-field distribution at a cross section of the entire model (including head) for case A′ [shown in Fig. 3(a)]. Note the low fields in the region marked as secondary. Also note that the plane of the coils are inclined toward each other by about 25°. (b) Variation of the H-field along the axis of the concentric loops [using Equation (2)] and the axis of the spiral (from FDTD). Curves at 5 and 10 MHz have been obtained with the head model without the implant, while the curve at 15 MHz has been obtained with the head model and the model of the implant. Note in the latter the dip in the H-field magnitude at the location of the secondary coil.

A comparison of the H-fields using (2) with that from FDTD simulations is shown in Fig. 9(b). Results for 5 and 10 MHz are without the implant in the head model and indicate the relative invariance of the H-field with the frequency in its reactive field and the relative transparency of the tissues to the magnetic fields at these frequencies. Results for these two frequencies show good agreement with the free-space formula-based result. A possible reason for the difference is the fact that the formula considers concentric loops of current as opposed to the spiral in the FDTD simulation. Fig. 9(a) and the third plot in Fig. 9(b) illustrate the effect of the secondary coil on the magnetic fields around the implant.

V. Results

The maximum E-field values were obtained in the insulation region around the secondary coil, which behaves like a short circuit where the fields are almost zero. The largest E-field values in the tissues were obtained in the peripheral regions of the head when the coil was closest to the forehead. Because of the discretization of the implant, the curved surfaces are jagged, which is further pronounced by subsequent rotations for the different orientations. Numerical errors due to staircasing [14] at tissue–implant and tissue–air interface and artifacts of the 2-equation–2-unknown method are the most likely causes for some single-voxel peaks. However, these local peaks are averaged out during the calculation of the 1-g SAR.

Fig. 10 illustrates the electric field, current density, and the SAR distribution for cases B and B′. The peak 1-g SAR values for the different cases are listed in Table II. Since it is not possible to obtain exact cubes of mass equal to 1 g, allowances of 10% (by weight) were made. Furthermore, for regions near the air interface, where the largest field values exist, the head boundary is very irregular, leading to incorporation of a large number or air voxels, which might lead to an incorrect estimation of the 1-g SAR. Therefore, to reduce the effect, while in-

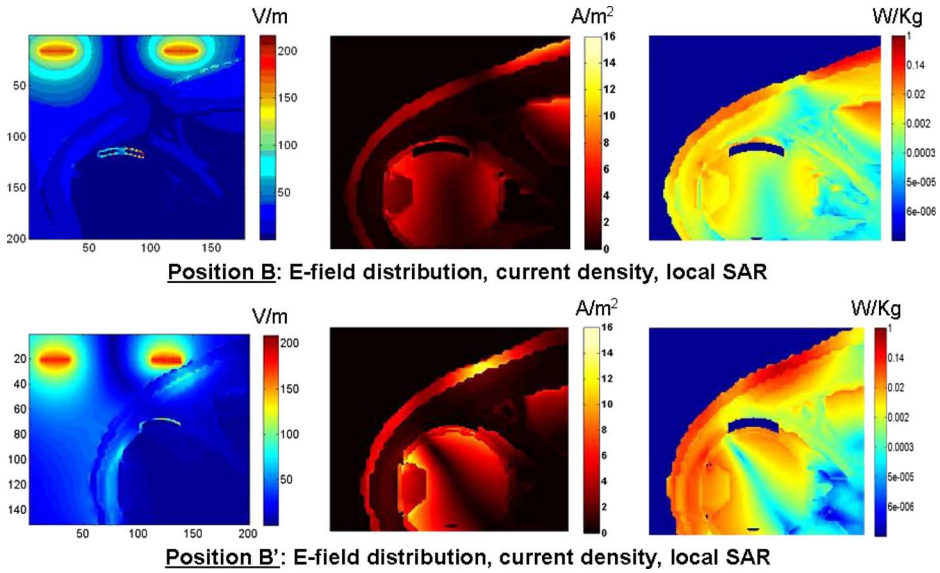

Fig. 10. E-fields, current density, and SAR along a transverse cross section of the head model (all values are single-voxel).

TABLE II
PEAK 1-g SAR AND AVERAGED CURRENT DENSITIES AT 10 MHz FOR PEAK PRIMARY COIL CURRENT OF 0.62 A

IEEE limit for SAR: 1.6 W/Kg ICNIRP limit for rms J: f/500=20 Am^{-2}		
Cases	peak 1-g SAR W/Kg	Current Density(J),Am^{-2} over 1 cm^2
A	0.12	6.4
B	0.08	5.2
C	0.08	5.2
A'	0.49	16.05
B'	0.11	7.7
C'	0.10	7.7

cluding most of the interface tissue voxels, it was decided to limit the maximum number of air voxels in the cube to 20% of the total number of voxels. Comparison with the IEEE standards [15] indicates that the telemetry system with a current of 0.62 A flowing in the primary coil in the presence of the human head and operating at 10 MHz is within safety limits. While the 10-g SAR has not been computed, it will be lower than the 1-g SAR, leading to compliance with the ICNIRP-imposed restriction of 2 W/kg over 10 g of tissue as well. Since the worst case is within the safety limits at 10 MHz, we will now concentrate on analyzing the electromagnetic effects of the telemetry system for different input parameters for the worst case orientation (position A').

In the near reactive field of a magnetic dipole, where the interaction with tissues is mainly by magnetic induction, the induced E-fields nearly scale with frequency ($\mathrm{E} \sim \mathrm{j}\omega\mathrm{B}$). This was verified for the model with simulations up to 20 MHz (Fig. 11).

During the design stage, which is often an iterative process, it is helpful to obtain the electromagnetic safety parameters such as the peak 1-g SAR quickly. This could be accomplished by scaling the fields. To illustrate this, first, the peak 1-g SAR was computed at several frequencies (Table III) between 2 and 20 MHz. Then, since the SAR $(\omega) \sim \sigma(\omega)\ |E|^2$, it is possible

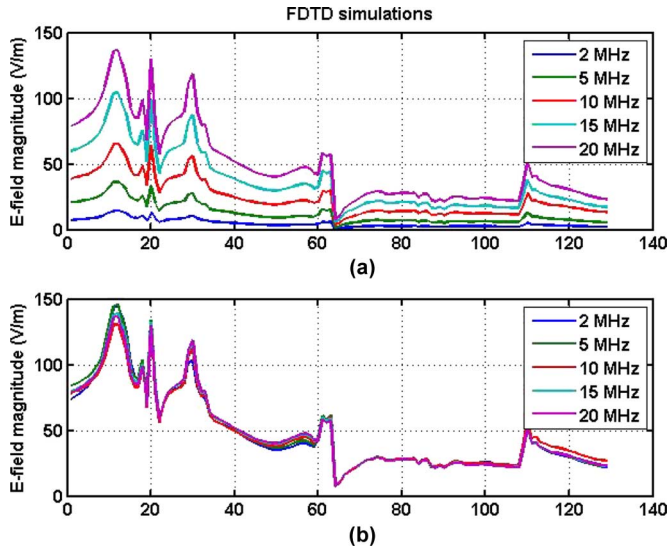

Fig. 11. (a) Variation of the E-field along a line parallel to the primary coil axis and through the head at various frequencies. (b) Curves at all frequency are scaled to that at 20 MHz to illustrate the minor variation in the profile of the magnetic field as a function of the frequency.

to obtain reasonable estimates by scaling the conductivity [12] and E-field (proportional to ω) from numerically computed values. Fig. 12 shows two curves. One is of the numerically computed peak 1-g SAR values at 2, 5, 10, 15, and 20 MHz. The second shows the 1-g SAR at all the frequencies scaled from 10 MHz (i.e., $\mathrm{error}_{10\ \mathrm{MHz}} = 0\%$). Intuitively, errors should be lower when scaling from nearer frequencies. For example, to estimate the peak 1-g SAR at 5 MHz, scaling from 10 MHz gives a 13% error (indicated in figure), while scaling from 2 MHz (not shown in figure) reduces the error to about 10%. Therefore, by using the computed values at the five frequencies, it is possible to estimate the peak 1-g SAR at any intermediate frequencies. Note that, in the above discussion, the tissue with the maximum contribution to the volume (for peak-1 g SAR) has been considered as being representative of

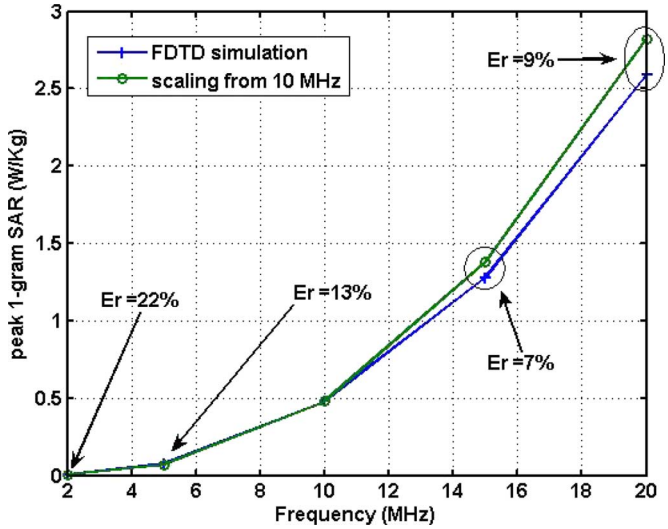

Fig. 12. Variation of the peak 1-g SAR with excitation frequency (for a primary coil current $\mathrm{I} = 0.62$ A) for case A′. 'Er' indicates the error due to scaling from 10 MHz.

TABLE III
PEAK 1-g SAR AND $J_{\max,\mathrm{rms}}$ WITH FREQUENCY FOR THE WORST CASE (A′) FOR PEAK PRIMARY COIL CURRENT OF 0.62 A

Frequency	peak 1-g SAR W/Kg	$J_{max,rms}$ $\mathrm{A}m^{-2}$
2 MHz	0.005	3.87
5 MHz	0.078	6.86
10 MHz	0.49	16.05
15 MHz	1.28	25.89
20 MHz	2.59	39.84

the volume or area. This assumption would not be valid if the region being considered was highly heterogeneous.

The current density distribution was similar to that of the SAR. Sclera, retina, and vitreous humor have relatively large conductivities, leading to higher current densities than outside the eye, except in the skin at the air interface (Fig. 10).

The root mean square (rms) current densities were obtained as averages over a cross section of 1 cm^2 perpendicular to the current flow, as outlined in the ICNIRP guidelines [7], and are mentioned in Table III. The maximum averaged rms currents $(J_{\max,\mathrm{rms}})$ were obtained around the skin region. Allowances and assumptions similar to those for the peak 1-g SAR were made.

The location of the $J_{\max,\mathrm{rms}}$ up to 10 MHz was at the same location in the muscle tissue (location M) under the skin, owing to its higher conductivity (Table I), even though the induced E-fields are lower (relative to skin). Also, since the conductivity of muscle varies little between 2 and 20 MHz (0.55 to 0.64), the variation of the $J_{\max,\mathrm{rms}}$ is almost linear (dashed curve in Fig. 13). A relatively larger increase in the conductivity of skin leads to the $J_{\max,\mathrm{rms}}$ occurring at skin at frequencies of 15 MHz and greater. However, as mentioned in the introduction, for frequencies greater than 10 MHz, induced current densities is not a safety criterion.

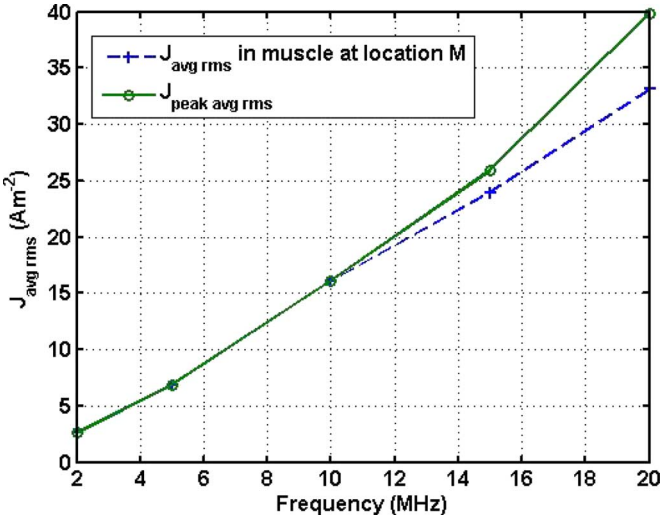

Fig. 13. Variation of the $J_{\max,\mathrm{rms}}$ with frequency for case A′.

VI. CONCLUSION

In this work, we have investigated, via FDTD simulations, the safety of the telemetry link investigated for use with the Second Sight Medical Products epi-retinal prosthesis system. A simple excitation scheme was used for the multiturn spiral primary coil, wherein ideal D-field sources were used. The accuracy of the source model has been verified both with an analytical model and experimentally. Different orientations and distances of the primary coil, based on the expected movement of the eye of the patient, were considered. For a normalized peak current of 0.62 A, the peak 1-g SAR for the worst-case orientation at 10 MHz was 0.49 W/Kg, and the peak rms current density averaged over an area of 1 cm^2 was 16.05 $\mathrm{A/m}^2$, which are both well within safety limits specified by IEEE and ICNIRP. It was verified that, at the considered frequencies, a simple scaling procedure can be used to obtain the E-field at different frequencies; from the computed values between 2 and 20 MHz, the peak 1-g SAR can be obtained for any frequency with an error of less than 10%. The $J_{\max,\mathrm{rms}}$ can also be obtained similarly within a similar error tolerance.

By interpolating, for the same current in the primary coil, the peak 1-g SAR limit of 1.6 W/Kg would be crossed around 16 MHz. Furthermore, at 10 MHz, the $J_{\max,\mathrm{rms}}$ of 20 $\mathrm{A/m}^2$ would be crossed for a primary coil current of about 0.78 A. The optimum frequency will ultimately be decided factoring in parameters such as coupling between the coils, induced current densities, and energy absorption in the tissues.

REFERENCES

[1] E. Margalit, M. Maia, J. D. Weiland, R. J. Greenberg, G. Y. Fujii, G. Torres, D. V. Piyathaisere, T. M. O'Hearn, W. Liu, G. Lazzi, G. Dagnelie, D. A. Scribner, E. de Juan, Jr., and M. S. Humayun, "Retinal prosthesis for the blind," *Survey Ophthalmology*, vol. 47, no. 4, pp. 335–356, 2002.

[2] J. D. Weiland, W. Liu, and M. S. Humayun, "Retinal prosthesis," *Annuv. Rev. Biomed. Eng.*, vol. 7, pp. 361–401, 2005.

[3] A. Y. Chow, M. T. Pardue, G. A. Peyman, and N. S. Peachey, "Development and application of subretinal semiconductor microphotodiode array," in *Vitreoretinal Surgical Techniques*, F. A. Peyman, S. A. Meffert, M. D. Conway, and F. Chou, Eds. London, U.K.: Martin Dunitz, Ltd, 2001, p. 576.

[4] J. Wyatt and J. F. Rizzo, "Ocular implants for the blind," *IEEE Spectrum*, vol. 33, no. 5, pp. 47–53, May 1996.
[5] G. Lazzi, "Thermal effects of implants," *IEEE Eng. Med. Bio. Mag.*, vol. 24, no. 5, pp. 75–81, Sep.–Oct. 2005.
[6] V. Singh, A. Roy, K. McClure, R. Dai, R. Agrawal, R. J. Greenberg, J. D. Weiland, M. S. Humayun, and G. Lazzi, "On the thermal elevation of a 60-electrode epi-retinal prosthesis for the blind," *IEEE Trans. Biomed. Circuits Syst.*, vol. 2, no. 4, pp. 289–300, Dec. 2008.
[7] ICNIRP Guidelines, "Guidelines for limiting exposure to time-varying electric, magnetic, and electromagnetic fields (up to 300 GHz)," *Health Phys.*, vol. 74, no. 4, pp. 494–522, 1998.
[8] S. C. DeMarco, G. Lazzi, W. Liu, J. D. Weiland, and M. S. Humayun, "Computed SAR and thermal elevation in a 0.25 mm 2-D model of the human eye and head in response to an implanted retinal stimulator—Part I: Models and methods," *IEEE Trans. Antennas Propagation*, vol. 51, no. 9, pp. 2274–2285, Sep. 2003.
[9] G. Lazzi, S. C. DeMarco, W. Liu, J. D. Weiland, and M. S. Humayun, "Computed SAR and thermal elevation in a 0.25 mm 2-D model of the human eye and head in response to an implanted retinal stimulator—Part II: Results," *IEEE Trans. Antennas and Propagation*, vol. 51, no. 9, pp. 2276–2295, Sep. 2003.
[10] K. Gosalia, J. Weiland, M. Humayun, and G. Lazzi, "Thermal elevation in the human eye and head due to operation of a retinal prosthesis," *IEEE Trans. Biomed. Eng.*, vol. 51, no. 8, pp. 1469–1477, Aug. 2004.
[11] The National Library of Medicine, "The Visible Human Project," 2000 [Online]. Available: http://www.nlm.nih.gov/research/visible/
[12] Italian National Research Council, "Dielectric properties of body tissue," 1997–2007 [Online]. Available: http://niremf.ifac.cnr.it/tissprop/
[13] K. P. Esselle and M. A. Stuchly, "Neural stimulation with magnetic fields: Analysis of induced electric fields," *IEEE Trans. Biomed. Eng.*, vol. 39, no. 7, pp. 693–700, Jul. 1992.
[14] M. A. Stuchly and T. W. Dawson, "Interaction of low-frequency electric and magnetic fields with the human body," *Proc. IEEE*, vol. 88, no. 5, pp. 643–664, 2000.
[15] *IEEE Standard for Safety Levels With Respect to Human Exposure to Radio Frequency Electromagnetic Fields, 3 KHz to 300 GHz*, IEEE Standard C95.1, 1999.
[16] E. Litvak, K. R. Foster, and M. H. Repacholi, "Health and safety implications of exposure to electromagnetic fields in the frequency range 300 Hz to 10 MHz," *Bioelectromagn.*, vol. 23, pp. 68–82, 2002.

Vinit Singh (S'05) received the B.Tech. degree in electronics and communication engineering from Indian Institute of Technology, Roorkee, India, in 2002; the M.S. degree in electronic materials and devices from the University of Cincinnati, Cincinnati, OH, in 2004; and the Ph.D. in electrical engineering from North Carolina State University, Raleigh, in May 2009.

He is currently a Project Scientist for a medical device startup in Chicago, IL, where he is working on wireless technologies for implantable devices and neuroanalgesics. His interests include antenna development for wireless power and communications, RFIDs, biomedical devices, and computational electromagnetics for dosimetric aspects of human interaction with EM fields.

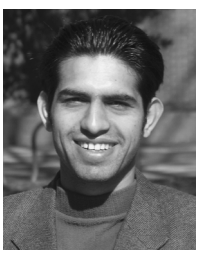

Amit Qusba received the B.Tech. degree in electronics and communications engineering from Indian Institute of Technology, Guwahati, India, in 2006.

Currently, he is pursuing the doctorate in electrical engineering at North Carolina State University, Raleigh. His research interests include computational electromagnetism, bioelectromagnetics, digital communication, and circuit design for wireless communications.

Arup Roy received the B.Tech. in instrumentation engineering from Indian Institute of Technology, Kharagpur, India, and the Ph.D. in biomedical engineering from the Johns Hopkins University, Baltimore, MD, where his thesis research was in the field of computational neuroscience.

He is presently working for Second Sight Medical Products, Inc., Sylmar, CA, as a Manager of Systems Engineering. His interests lie in the field of neural prostheses and medical device design and development.

Richard A. Castro received the B.S. degree in electrical engineering from California Institute of Technology, Pasadena, in 2000, and the M.S. degree in bioengineering from the University of California, San Diego, in 2002.

As a student at the University of California, San Diego, he contributed to the development of a telemetry instrumentation system for the continuous monitoring of metabolic activity. He is currently a Principal Engineer at Second Sight Medical Products, Inc., Sylmar, CA, specializing in electronic hardware design for both embedded and RF systems.

Kelly McClure (M'91) received the M.S. degree in computer engineering/bioengineering from Carnegie Institute of Technology, Pittsburgh, PA.

He is Senior Director of Systems Research and Development at Second Sight Medical Products, Inc., Sylmar, CA. His interest is in active implantable medical device systems for neurostimulation and neuromoduation as well as sensing of peripheral and central nervous system signals.

Mr. McClure is a Member of the Association for Research in Vision and Ophthalmology (ARVO).

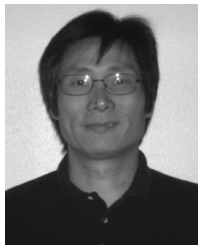

Rongching Dai (M'00) received the M.Sc. degree in neuroscience and the M.S.E.E. degree from University of Alberta, Edmonton, AB, Canada in 1996 and 1997, respectively.

He was involved in researches in gait assistance with Functional Electrical Stimulation (FES) for spinal cord injured patients before joining Second Sight Medical Products, Inc., Sylmar, CA, in 1999, where he has been the Lead Engineer developing the ASIC chip for epi-retinal stimulators. His research interests include low-power design and safety protocols for inductively powered implant electronic devices.

Robert J. Greenberg (M'87) received the degree in technical electronics from Nassau Technical Institute, Bahamas, in 1985; the B.S. degree in electrical and biomedical engineering from Duke University, Durham, NC, in 1990; and the Medical degree from The Johns Hopkins University School of Medicine, Baltimore, MD, in 1998.

From 1991 to 1997, he conducted animal and human trials demonstrating the feasibility of retinal electrical stimulation in patients with *Retinitis Pigmentosa*. This work was done at the Wilmer Eye Institute at The Johns Hopkins Hospital, Baltimore, MD, and led to the granting of his Ph.D. in 1997 from the Johns Hopkins Biomedical Engineering Department. He sits on the Board of Directors of the Los Feliz Arts Charter and the So-CalBio and is Chairman of the Alfred E. Mann Foundation, Santa Clara, CA. He has been the President and CEO of Second Sight Medical Products, Inc., Sylmar, CA, since its inception in 1998. Prior to the formation of Second

Sight, he co-managed the Alfred E. Mann Foundation. From 1997 to 1998, he served as a Medical Officer and Lead Reviewer for IDEs and 510(k)s at the Office of Device Evaluation at the U.S. Food and Drug Administration in the Neurological Devices Division. He also has biosensor and microsensor fabrication experience from work and teaching at the Whittaker Sensors Laboratory, Johns Hopkins University. He has started several other small companies, including one called "Campus Security" where he designed, manufactured, and marketed an electronic intercom security system called TELEKEY. These intercoms are currently in use in every dormitory at Princeton University, Princeton, NJ; Duke University, Durham, NC; and several other universities across the US.

James D. Weiland (SM'08) received the B.S. degree, the M.S. degree in biomedical engineering, the M.S. degree in electrical engineering, and the Ph.D. degree in biomedical engineering from the University of Michigan, Ann Arbor, in 1988, 1993, 1995, and 1997, respectively.

He spent four years in industry with Pratt & Whitney Aircraft Engines, East Hartford, CT, before returning to Michigan for graduate school. He joined the Wilmer Ophthalmological Institute, The Johns Hopkins University, Baltimore, MD, in 1997 as a Post-Doctoral Fellow and was appointed Assistant Professor of ophthalmology in 1999. He was appointed Assistant Professor at the Doheny Eye Institute, Keck School of Medicine, University of Southern California, Los Angeles, in 2001 and is currently an Associate Professor of Ophthalmology and Biomedical Engineering. His research interests include retinal prostheses, neural prostheses, electrode technology, visual evoked responses, and implantable electrical systems.

Dr. Weiland is a Member of the Biomedical Engineering Society, Sigma Xi, and the Association for Research in Vision and Ophthalmology.

Mark S. Humayun (M'97) received the B.S. degree from Georgetown University, Washington, DC, in 1984, the M.D. degree from Duke University, Durham, NC, in 1989, and the Ph.D. degree from the University of North Carolina, Chapel Hill, in 1994.

He completed an ophthalmology residency at Duke Eye Center, Durham, NC, and fellowships in both vitreoretinal and retinovascular surgery at The Johns Hopkins Hospital, Baltimore, MD. He stayed on as faculty at The Johns Hopkins University, Baltimore, MD, where he rose to the rank of Associate Professor before moving to the University of Southern California (USC), Los Angeles, in 2001. He is currently a Professor of Ophthalmology, Biomedical Engineering, and Cell and Neurobiology at the Doheny Eye Institute, Keck School of Medicine, USC. He is the Director of the National Science Foundation BioMimetic MicroElectronic Systems Engineering Research Center, Los Angeles, a national center of excellence aimed at researching and developing micro and nanotechnology to mimic and replace damaged and diseased systems in the human body. He is also the Director of the Department of Energy Artificial Retina Project, which is a unique consortium of five Department of Energy laboratories, five universities, as well as industry. His research projects focus on the treatment of the most debilitating and challenging eye diseases through advanced engineering. Leading a team of more than 30 faculty and 200 students from 15 different institutes, he is focused on developing therapies for: 1) retinal degenerations such as retinitis pigmentosa; 2) macular degenerations such as age-related macular degeneration; 3) retinovascular diseases such as vein occlusions; 4) diabetic retinopathy; as well as 5) glaucoma. He has authored more than 120 peer-review scientific papers and chapters. He has been invited to participate as a guest speaker an equally impressive number of times in more than 20 countries around the world. His work on the intraocular retinal prosthesis ("artificial vision") has been featured prominently in more than 500 newspapers and television programs, throughout the United States and abroad. He also holds 11 issued patents, with numerous patents pending. His work has spawned three companies to date.

Dr. Humayun is a Member of 11 academic organizations, including the Biomedical Engineering Society, the Association for Research in Vision and Ophthalmology, the American Society of Retinal Specialists, the Retina Society, the American Ophthalmological Society and the American Academy of Ophthalmology, and Biomedical Engineering in Medicine and Biology. He has also been a key member on a number of national academies panels. He is well-recognized by his peers both as a top ophthalmologist as well as a leading biomedical engineer. He has been voted as one of the best doctors in America and has received numerous research awards. For his outstanding contributions to engineering, He was named the Innovator of the Year in 2005 by *R&D Magazine*.

Gianluca Lazzi (S'94–M'95–SM'99–F'08) received the Dr.Eng. degree in electronics from the University of Rome "La Sapienza," Rome, Italy, in 1994, and the Ph.D. degree in electrical engineering from the University of Utah, Salt Lake City, in 1998.

He is currently a Professor with the Department of Electrical and Computer Engineering, North Carolina State University (NCSU), Raleigh. He was an Assistant Professor at NCSU from 1999 to 2003 and an Associate Professor from 2003 to 2006. He has been a Visiting Researcher with the Italian National Board for New Technologies, Energy, and Environment (ENEA) (1994), a Visiting Researcher with the University of Rome "La Sapienza" (1994–1995), and a Research Associate (1995–1998) and Research Assistant Professor (1998–1999) with the University of Utah. He has authored or co-authored over 100 international journal papers or conference presentations on implantable devices, medical applications of electromagnetic fields, antenna design, FDTD modeling, dosimetry, and bioelectromagnetics.

Dr. Lazzi is the past Chair of Commission K (Electromagnetics in Biology and Medicine) of the U.S. National Committee of the International Union of Radio Science (URSI). He is the Technical Program Chair of the 2009 IEEE Antennas and Propagation-URSI International Symposium (Charleston, SC). He was the recipient of the 1996 "Curtis Carl Johnson Memorial Award" for the best student paper presented at the 18th Annual Technical Meeting of the Bioelectromagnetics Society (BEMS), a 1996 URSI "Young Scientist Award," a 2001 Whitaker Foundation Biomedical Engineering Grant for Young Investigators, a 2001 National Science Foundation (NSF) CAREER Award, a 2003 NCSU Outstanding Teacher Award, the 2003 NCSU Alumni Outstanding Teacher Award, the 2003 ALCOA Foundation Engineering Research Award, the 2006 H. A. Wheeler Award from the IEEE Antennas and Propagation Society for best application paper published in the IEEE TRANSACTIONS ON ANTENNAS AND PROPAGATION in 2005, and a Best Paper Award at the IEEE GlobeCom conference in 2008. He has been an Associate Editor for the IEEE ANTENNAS AND WIRELESS PROPAGATION LETTERS (2001–2007) and served as a Guest Editor for the "Special Issue on Biological Effects and Medical Applications of RF/Microwaves" of the IEEE TRANSACTIONS ON MICROWAVE THEORY AND TECHNIQUES in 2004. He is currently the Editor-in-Chief of the IEEE ANTENNAS AND WIRELESS PROPAGATION LETTERS.